Electrochimica Acta 210 (2016) 874–879

Contents lists available at ScienceDirect

Electrochimica Acta

journal homepage: www.elsevier.com/locate/electacta

Employing inorganic/organic hybrid interface layer to improve electron transfer for inverted polymer solar cells

Zhiqi Li[a], Xinyuan Zhang[a], Shujun Li[a,c], Chunyu Liu[a], Zhihui Zhang[a], Jinfeng Li[a], Liang Shen[a,b], Wenbin Guo[a,*], Shengping Ruan[a,*]

[a] State Key Laboratory on Integrated Optoelectronics, College of Electronic Science and Engineering, Jilin University, 2699 Qianjin Street, Changchun 130012, People's Republic of China
[b] Department of Mechanical and Materials Engineering and Nebraska Center for Materials and Nanoscience, University of Nebraska–Lincoln, Lincoln, Nebraska 68588-0656, USA
[c] Changchun Institute of Optics, Fine Mechanics and Physics, Chinese Academy of Sciences, 3888 Eastern South Lake Road, Changchun, 130033, People's Republic of China

ARTICLE INFO

Article history:
Received 16 March 2016
Received in revised form 2 June 2016
Accepted 4 June 2016
Available online 6 June 2016

Keywords:
polymer solar cells
charge transfer
exciton dissociation
work function
morphology

ABSTRACT

The performance of inverted polymer solar cells (PSCs) was enhanced by introducing TiO_x and poly(9,9-dioctylfluorenyl-2,7-diyl) (PFD) as a hybrid buffer layer. Surface morphology and work function measurement demonstrated that PFD interlayer eliminated the defects and traps from TiO_x surface and acted as an efficient charge transport matrix, resulting in enhanced electron mobility and reduced interface resistance. Therefore, the employment of TiO_x/PFD composite layer improved to extract electron from active layer to ITO electrode and dramatically increased device efficiency from 5.717% to 7.272%, accounting for a 27.2% increase. The achieved high device efficiency, low-cost materials, and solution processes of TiO_x/PFD layer provide a promising candidate for realizing high performance photovoltaic devices.

1. Introduction

Polymer solar cells (PSCs) are exhibiting considerable promise for commercial applications because of considerable advantages in the realization of a low-cost, printable, flexible, and lightweight renewable energy source [1–8]. However, the overall performance of PSCs is still limited by many factors, such as insufficient light absorption of the photolayer, poor nanomorphology, and low charge carrier mobility [9–12], further advancement could be achieved by solving these problems. Generally, photovoltaic conversion is composed of four processes: (1) photons absorption and excitons generation; (2) excitons diffusion in active layer; (3) excitons dissociation; (4) free carriers transport and extraction [13,14]. Usually, the materials used in PSCs have a low dielectric constant, and the Coulomb force of charge carriers is larger in PSCs than that in silicon solar cells, which leads to a tightly binding hole–electron pair (exciton) after light excitation rather than free charge carriers. Also, exciton recombination often occurs in the process of diffusion, dissociation, and collection. An effective method to reduce exciton recombination and improve injection efficiency is to employ the proper electrodes with matched work functions. Therefore, inorganic buffer layers including TiO_x, MoO_x, and ZnO between the active layer and cathode have been used to reduce carrier accumulation on the electrode in past few years [15–22]. Ideally, PSCs should have balanced charge transfer and collection to ensure high charge extraction capacity of electrodes, which requires a good interface contact between various layers. However, rebellious nanomorphology of inorganic layer makes it difficult to attain optimized interface with polymer layer to enhance interconnected pathways for charge transport, as well as decrease charge recombination [23–25]. To address the interface issues, numerous studies have been implemented, such as rational design of dopant molecules [26], conjugated polyelectrolytes [27], and self-assemble molecule [28]. However, the utilization of the amphiphilic materials as the interfacial layer to improve coherence of active layer and buffer layer is rarely reported.

In this paper, poly(9,9-dioctylfluorenyl-2,7-diyl) (PFD) was introduced as a modification layer on TiO_x to achieve high-

* Corresponding authors.
E-mail addresses: guowb@jlu.edu.cn, oedcad@gmail.com (W. Guo).

http://dx.doi.org/10.1016/j.electacta.2016.06.022
0013-4686/

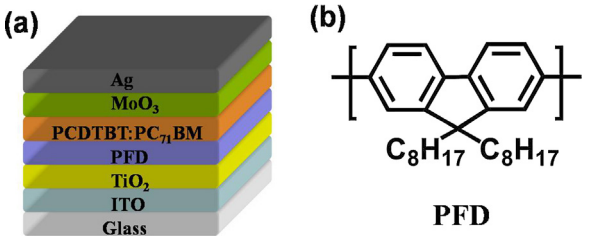

Fig 1. (a) The device structure of the inverted polymer solar cell, (b) the molecule structure of PFD.

efficiency for inverted PSCs. The sensitized inorganic/organic composite interlayer was estimated by the surface morphology measurement and the work function analysis. It is worthy noting that PFD perfected TiO_x nanomorphology and offered effective interconnected pathways for electron transfer. PFD capping layer eliminated the defects and traps from TiO_x surface and acted as an efficient charge transport matrix. Hence, charge transfer rates from excited polymer molecules to TiO_x can remarkably be accelerated upon illumination when they are chemically attached. As a result, the photocurrent density (J_{sc}) and the fill factor (FF) of PSCs were increased from 12.726 mA/cm^2 to 13.682 mA/cm^2 and 52.549% to 61.29% respectively, leading to a greatly enhanced power conversion efficiency (PCE) from 5.717% to 7.272%.

2. Experimental

The device structure of the inverted PSCs and the chemical structure of the PFD are schematically presented in Fig. 1. PCDTBT and $PC_{71}BM$ were purchased from 1-Material Chemscitech Inc. and Lumitec Corp. respectively, which were used without purification. In order to demonstrate the effect of PFD, the device with configuration of ITO (180 nm)/TiO_2(40 nm)/PFD/PCDTBT:$PC_{71}BM$ (~100 nm)/MoO_3 (4 nm)/Ag (100 nm) was fabricated. Firstly, a pretreatment commercial ITO based glass was cleaned by detergent, deionized water, acetone, and isopropanol in turn. Secondly, a 40 nm electron transport layer of TiO_x was prepared by sol-gel and spin-coated on cleaned ITO substrates. Thirdly, PFD dissolved in tetrahydrofuran with the concentration of 1000 ppm was spin-coated on top of the TiO_x thin film, and then annealed at 80 °C for 10 min in air. The corresponding devices made with different thickness of PFD were labeled as Device A (0 nm), Device B (1 nm), Device C (3 nm), Device D (8 nm), and Device E (11 nm), respectively. PCDTBT (7 mg) and $PC_{71}BM$ (28 mg) blending were dissolved in 1 mL 1,2-odichlorobenzene solvent. The mixed solution was then spun-cast onto the precoated PFD layer to form the active layer, whose thickness is ~100 nm. Then, the active layer was annealed at 70 °C for 20 min. Finally, the device fabrication was completed by thermal evaporation of a MoO_x buffer layer (4 nm) and an Ag anode (100 nm) layer at a vacuum of 10^{-6} torr. The evaporator is BOC Edwards Auto 306, and the active layer area of the device is defined by a shadow mask of 2 mm × 3.2 mm. The photocurrent density-voltage (J-V) characteristic was performed under 100 mW/cm^2 with an AM 1.5 G condition. The light intensity was precisely calibrated by a calibrated silicon solar cell. The morphologies of the thin films were characterized by atomic force microscopy (AFM) in tapping mode (Dimension icon scanasyst). IPCE spectra of the devices were characterized a commercial photo-modulation spectroscopic setup (DSR100UV-B). J-V characteristics of electron-only device was measured with the device structure of ITO/TiO_x/PFD/PCDTBT:$PC_{71}BM$/BCP/Ag and ITO/TiO_x/PCDTBT:$PC_{71}BM$/BCP/Ag. J-V characteristic of the diodes was carried out with the structures of ITO/TiO_x/Ag and ITO/TiO_x/PFD/Ag [29–31].

3. Results and discussion

Fig. 2(a) exhibits J–V characteristics of PSCs with TiO_x (Device A) and various thickness of PFD coating TiO_x as buffer layers. As expected, the optimal device (Device C) with TiO_x/PFD interfacial layer indicated a J_{sc} of 13.682 mA cm^{-2}, a FF of 61.29%, and a V_{oc} of 0.867 V, leading to a PCE of 7.272%. By contrast, the best performance of the control device (Device A) with TiO_x transport layer owns a PCE of 5.717%, including a V_{oc} of 0.855 V, a FF of 52.54%, and a J_{sc} of 12.727 mA cm^{-2}. The detailed parameters of all fabricated devices are summarized in Table 1, which are typical average of 32 devices. To investigate the operation mechanism of TiO_x/PFD based devices, the incident photon-to-electron conversion efficiency (IPCE) is shown in Fig. 2(b). It can be seen that

Table 1
The detailed performance parameters of all PSC devices without and with different thickness of PFD layers.

Thickness of PFD	Device	V_{oc} (V)	J_{sc} (mA/cm^2)	FF (%)	PCE (%)
0 nm	A	0.855	12.726	52.54	5.717
1 nm	B	0.861	13.272	59.18	6.755
3 nm	C	0.867	13.682	61.29	7.272
8 nm	D	0.863	12.597	58.49	6.368
11 nm	E	0.826	12.413	53.09	5.440

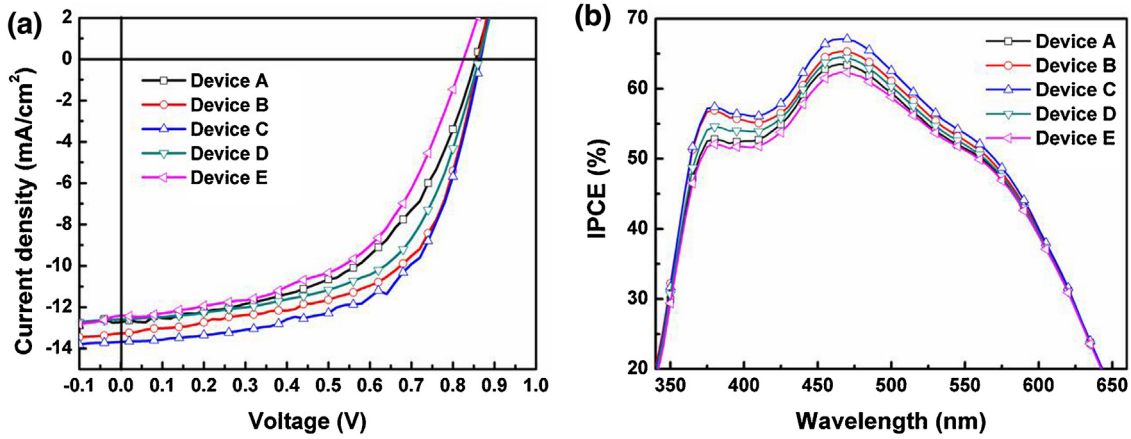

Fig. 2. (a) J–V characteristics and (b) IPCE of all PSCs without and with different thickness of PFD.

Device C demonstrates a higher IPCE throughout the visible range from 380 to 580 nm, and the peak value locates in the band of 475 nm. Thus, Device C possesses a high short-circuit density. The complete parameters comparison of Device A and Device C, including V_{oc}, FF, J_{sc}, and PCE were summarized in Fig. 3, and the optimized devices achieved comprehensive advantages. The introduction of the PFD interfacial layer could match the energetic alignment and perfect TiO_x nanomorphology. Meanwhile, the optimised interface would eliminat the defects and traps from the surface of TiO_x and act as an efficient charge collection matrix to reduce the contact resistance. Hence, these effects could provide plenty of interconnected pathways for charge transport [32–34].

In order to deeply explore the effect of PFD capping layer on the energy alignment, the changes of the work-functions (WF) induced by PFD layer were obtained using a Kelvin probe system (KP 6500 Digital Kelvin probe, McAllister Technical Services Co., Ltd.). It is well known that WF of the cathode and the lowest unoccupied molecular orbital (LUMO) of the PCBM must be well matched to form a good Ohmic contact, which is beneficial to balance charge transfer and minimize contact resistance. As shown in Fig. 4, the conduction band of TiO_x and PCBM are −4.2 eV and −3.8 eV, and the WF of the PFD and TiO_x are −4.2 eV and −4.6 eV, respectively

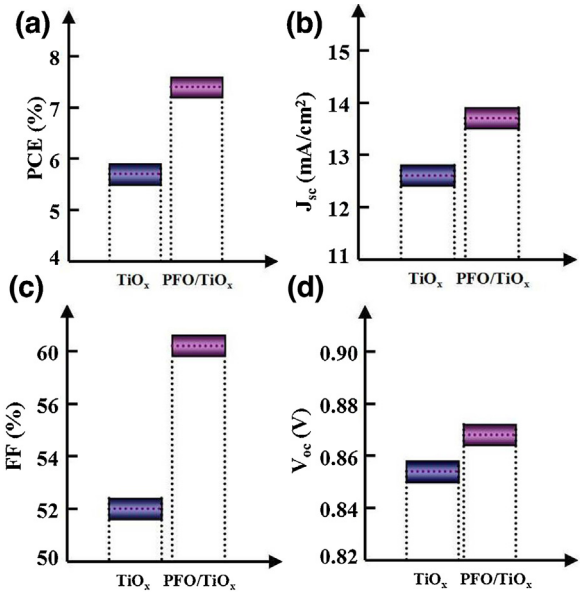

Fig. 3. The photovoltaic parameters comparison of control and optimal devices including (a) V_{oc}, (b) J_{sc}, (c) FF, and (d) PCE.

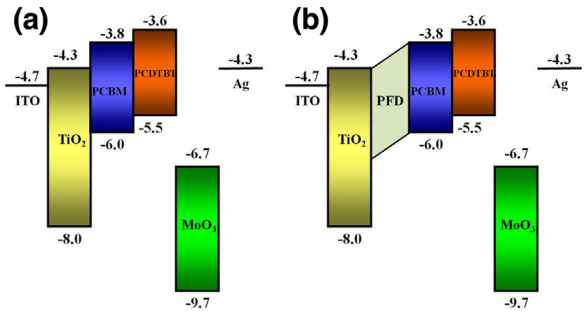

Fig. 4. Scheme energy levels of inverted polymer solar cells with (a) TiO_x and (b) TiO_x/PFD as electron transport layer.

[35]. It indicates that the PFD capping layer provides a bridge between the LUMO of PCBM and the conduction band of TiO_x. Therefore, the incorporation of PFD coating layer improved the energy alignment tuning between the WF of ITO and the LUMO of PCBM, leading to a decreased energy potential. Consequently, the energy tuning greatly accelerated charge transfer from excited organic molecules to inorganic electrode, resulting in increased charge collection.

As is well-known, the performance of PSCs depends on many factors, and the film morphology plays an important role on the device performance. Generally, morphology of the film can be adjusted by controlling the spin-casting solvent, the solution concentration, the controlled phase separation, and crystallization induced by thermal annealing [36]. To reveal the function of the PFD coating layer on TiO_x surface, the film nanomorphology was tested by atomic force microscopy (AFM). Fig. 5 shows the AFM topographic images of bare TiO_x film as well as capping with different thickness of PFD layer. Bare TiO_x film shows a root-mean-square (RMS) value of 0.52 nm, and the RMS values of TiO_x/PFD films slightly increased to 1.74 nm (Device B), 2.23 nm (Device C), and 2.79 nm (Device D). PFD capping TiO_x resulted in a relative enhancement of roughness in the interfacial partial area, which enhanced domain sizes to improve the contact between TiO_x and active layer. Therefore, improved TiO_x nanomorphology and increased interconnected pathways accelerated electron transport to the bottom-ITO electrode. Especifically, the reformed interfacial crystallinity and the formation of tight nanoscale domains led to a close contact, reducing the interface resistance. Additionally, the evenly distributed PFD layer filled the ditch and decreased interfacial charge trammel, decreasing charge recombination probability. Meanwhile, conductive PFD layer could also worked as efficient charge collection matrix, which penetrated around the fullerene clusters and the polymer-skin, increasing the diffusion length in the process of electron transport. Improved interfacial coherence and electrical conductivity mentioned above reduced the energy barrier at the TiO_x and active layer interface and decreased the energy loss within the TiO_x itself, thus a higher photocurrent was developed [37].

To further understand the effect of matched energy alignment and improved film morphology induced by the PFD layers, the dark J-V characteristics of inverted PSCs with and without PFD layers were measured. As indicated in Fig. 6(a), devices with the PFD layers shows smaller leakage current at negative voltages and low positive voltages, and rapidly increased current in the space charge limited current dominated regime was achieved, leading to an improved rectifying property. Furthermore, the electrical impedance spectroscopy (EIS) of all devices was presented in Fig. 6(b). It can be seen that Device C exhibits slightly lower charge transfer resistance than Device A, suggesting that TiO_x/PFD buffer layer effectively facilitates electron transport from the active layer to ITO. The enhancement of electron transport and decrease of contact resistance are also reflected in the increased FF.

To deeply investigate the role of PFD layer on the mechanism of electron transport for the control and optimal devices, the photocurrent density (J_{ph})—the effective voltage (V_{eff}) is calculated and drawn in Fig. 7(a). Herein, $J_{ph} = J_L - J_D$, $V_{eff} = V_o - V$, J_L and J_D are the current densities under illumination and in dark, respectively. V is the applied voltage and V_o is the compensation voltage at $J_{ph} = 0$ [38]. J_{ph} increases linearly with V_{eff} at $V_{eff} < 0.1$ V, and slope shows that the maximum exciton generation rate (G_{max}) of PFD capping PSCs is higher than the control device. Therefore, interface modification increases the electron transport and collection, leading to an enhanced exciton dissociation probability [P(E,T)] (Fig. 7(b)). Herein, $P(E,T) = J_{ph}/J_{sat}$, where J_{sat} is the saturation photocurrent density. J_{ph} tends to saturate at $V_{eff} > 0.8$ V, and a higher J_{ph} usually implies a larger charge extraction efficiency,

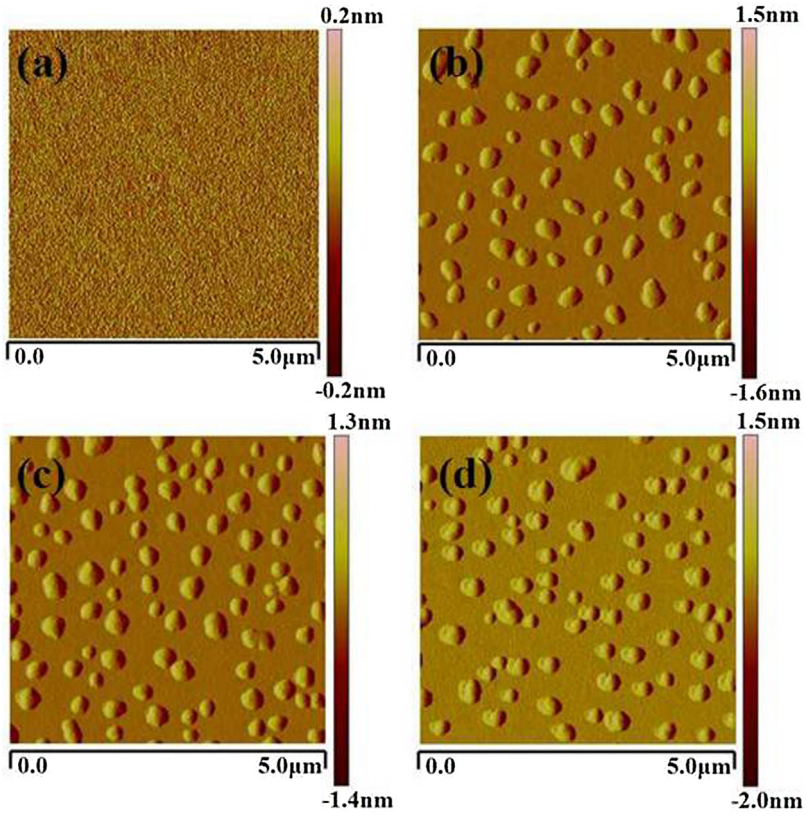

Fig. 5. AFM images of (a) TiO_x and TiO_x capped with different thickness of PFD layer, (b) TiO_x/PFD (1 nm), (c) TiO_x/PFD (3 nm), and (d)TiO_x/PFD (8 nm).

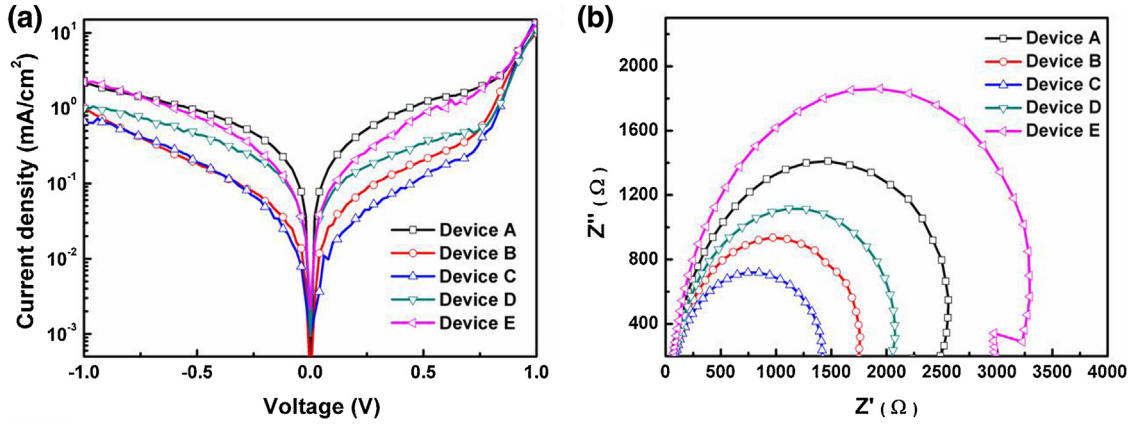

Fig. 6. (a) J-V characteristics and (b) impedance spectra of all polymer solar cells in dark.

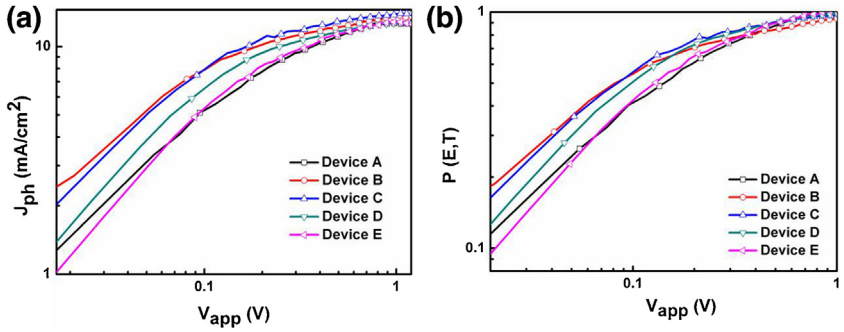

Fig. 7. (a) Photocurrent density (J_{ph}), and (b) exciton dissociation probability [P(E,T)] plotted with respect to effective bias (V_{eff}) for the reference and PFD capping devices.

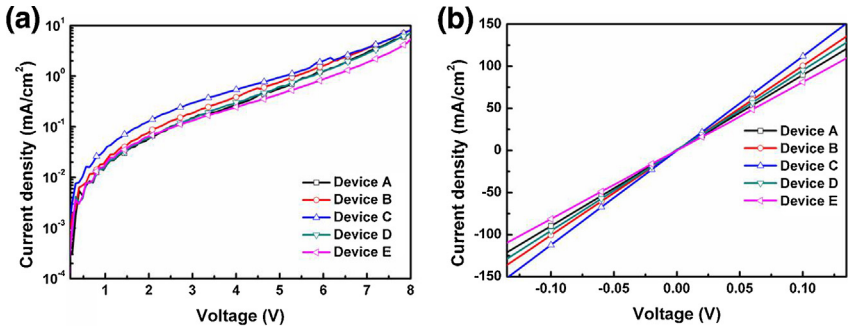

Fig. 8. (a) J-V characteristics of electron-only device, (b) J-V characteristic of the diodes with the structures of ITO/TiO_x/Ag and ITO/TiO_x/PFD/Ag.

accounting for a relatively increased FF and J_{sc} for PFD capping devices [39,40].

For the purpose of directly verifying the effect of PFD capping layer on the electron transport properties, single-electron devices were fabricated and represented in Fig. 8(a). It indicates that the incorporation of PFD made a contribution to the enhancement of electron mobility, leading to a higher J_{sc} and FF. We extracted electron mobility at a typical applied voltage of 1 V using the space-charge limited circuit model [41–43]. For Device A with pristine TiO_2 layer and the optimal Device C, electron mobilities were calculated to be $2.36 \times 10^{-5}\,cm^2\,V^{-1}\,s^{-1}$ and $2.8 \times 10^{-5}\,cm^2\,V^{-1}\,s^{-1}$, respectively. Meanwhile, the J-V characteristic of the diodes with the structures of ITO/TiO_2/Ag and ITO//TiO_2/PFD/Ag were investigated. The electrical conductivity is calculated by the following equation: $\delta = Gd/A$, where δ is the electrical conductivity, d is thickness of the thin film, and A is the device area, G is the conductance which can be derived from slope of *J-V* curve. The calculated electrical conductivity are 5.6×10^{-4} S/m (Device A) and 8.8×10^{-4} S/m (Device C), respectively. These results suggest that PFD capping layer can enhance electrical conductivity of cathode buffer layer and facilitate charge transport through TiO_2 layer to ITO electrode.

4. Summary

In conclusion, the performance enhancement of inverted PSCs was achieved via introducing PFD to cover TiO_x buffer layer. The efficiency of PSCs was increased from 5.717% up to 7.272%, accouting for a 27.2% enhancement. After PFD layer was employed, the better matching energy alignment between PFD and $PC_{71}BM$ and improved nanoscale morphology were achieved, which facilitated charge carriers collection from photoactive layer and decreased unwanted charge recombination, resulting in an enhanced PCE, FF, and J_{sc}. Our study provides an effective approach to realize high performance PSCs.

Acknowledgments

The authors are grateful to National Natural Science Foundation of China (61275035, 61370046, 11574110), Project of Science and Technology Development Plan of Jilin Province (20130206075SF), the Opened Fund of the State Key Laboratory on Integrated Optoelectronics (IOSKL2013KF10).

References

[1] S.E. Shaheen, C.J. Brabec, N.S. Sariciftci, F. Padinger, T. Fromherz, J.C. Hummelen, 2.5% efficient organic plastic solar cells, Appl. Phys. Lett. 78 (2001) 841–843.
[2] H.H. Liao, L.M. Chen, Z. Xu, G. Li, Y. Yang, Highly efficient inverted polymer solar cell by low temperature annealing of Cs_2CO_3 interlayer, Appl. Phys. Lett. 92 (2008) 173303.
[3] M. Andersen, J.E. Carle, N. Cruys-Bagger, M.R. Lilliedal, M.A. Hammond, B. Winther-Jensn, F.C. Krebs, Transparent anodes for polymer photovoltaics: oxygen permeability of PEDOT, Sol. Energy Mater. Sol. Cells 91 (2007) 539–543.
[4] K.S. Lee, J.A. Lee, B.A. Mazor, S.R. Forst, Transforming the cost of solar-to-electrical energy conversion: integrating thin-film GaAs solar cells with non-tracking mini-concentrators, Light: Sci. Appl. 4 (2015) e288.
[5] S.K. Hau, H.L. Yip, N.S. Baek, J. Zou, K. O'Malley, A.K.Y. Jen, Air-stable inverted flexible polymer solar cells using zinc oxide nanoparticles as an electron selective layer, Appl. Phys. Lett. 92 (2008) 253301.
[6] C. Edwards, A. Arbabi, G. Popescu, L.L. Goddard, Highly efficient inverted polymer solar cell by low temperature annealing of Cs_2CO_3 interlayer, Light: Sci. Appl. 1 (2012) e30.
[7] G. Yu, J. Gao, J.C. Hummelen, F. Wudl, A.J. Heeger, Polymer photovoltaic cells: enhanced efficiencies via a network of internal donor-acceptor heterojunctions, Science 270 (1995) 1789–1791.
[8] F.C. Krebs, S.A. Gevorgyan, J. Alstrup, A roll-to-roll process to flexible polymer solar cells: model studies, manufacture and operational stability studies, J. Mater. Chem. 9 (2009) 5442–5451.
[9] C.J. Brabec, S. Gowriasnker, Jonathan J.M. Halls, D. Laird, S.J. Jia, S.P. Williams, Polymer–Fullerene Bulk–Heterojunction Solar Cells, Adv. Mater. 22 (2010) 3839–3856.
[10] L.Y. Lu, Z.Q. Luo, T. Xu, L.P. Yu, Cooperative plasmonic effect of Ag and Au nanoparticles on enhancing performance of polymer solar cells, Nano Lett. 13 (2013) 59–64.
[11] R.A. Taylor, T. Otanicar, G. Rosengarten, Nanofluid-based optical filter optimization for PV/T systems, Light: Sci. Appl. 1 (2012) e34.
[12] Y.H. Su, Y.F. Ke, S.L. Cai, Q.Y. Yao, Surface plasmon resonance of layer-by-layer gold nanoparticles induced photoelectric current in environmentally-friendly plasmon-sensitized solar cell, Light: Sci. Appl. 1 (2012) e14.
[13] S.H. Park, A. Roy, S. Beaupre, S. Cho, N. Coates, J.S. Moon, D. Moses, M. Leclerc, K. Lee, A.J. Heeger, Bulk heterojunction solar cells with internal quantum efficiency approaching 100%, Nature Photonics 3 (2009) 297–302.
[14] B. Qi, J.Z. Wang, Fill factor in organic solar cells, Phys. Chem. Chem. Phys. 15 (2013) 8972–8982.
[15] C. Chen, F.M. Li, Improving the efficiency of ITO/nc-TiO_2/CdS/P3HT:PCBM/PEDOT:PSS/Ag inverted solar cells by sensitizing TiO_2 nanocrystalline film with chemical bath-deposited CdS quantum dots, Nanoscale Research Letters 8 (2013) 1–7.
[16] H. Choi, J.S. Park, E. Jeong, G.H. Kim, B.R. Lee, S.O. Kim, M.H. Song, H.Y. Woo, J.Y. Kim, Combination of titanium oxide and a conjugated polyelectrolyte for high performance inverted-type organic optoelectronic devices, Adv. Mater. 23 (2011) 2759–2763.
[17] S.H. Liu, P. You, J.H. Li, J. Li, C.S. Lee, B.S. Ong, C. Surya, F. Yan, Enhanced efficiency of polymer solar cells by adding a high-mobility conjugated polymer, Energy Environ. Sci 8 (2015) 1463–1470.
[18] Y. Zhang, H.Q. Zhou, J. Seifter, L. Ying, A. Mikhailovsky, Alan J. Heeger, Guillermo C. Bazan, T.Q. Nguyen, Molecular doping enhances photoconductivity in polymer bulk heterojunction solar cells, Adv. Mater. 25 (2013) 7038–7044.
[19] F. Deschler, E. Da Como, T. Limmer, R. Tautz, T. Godde, M. Bayer, E. von Hauff, S. Yilmaz, S. Allard, U. Scherf, J. Feldmann, Reduced charge transfer exciton recombination in organic semiconductor heterojunctions by molecular doping, Phys. Rev. Lett. 107 (2011) 127402.
[20] X. Liu, W. Wen, G.C. Bazan, Post-deposition treatment of an arylated-carbazole conjugated polymer for solar cell fabrication, Adv. Mater. 24 (2012) 4505–4510.
[21] X.C. Li, F.X. Xie, S.Q. Zhang, J.H. Hou, W.C.H. Choy, MoO_x and V_2O_x as hole and electron transport layers through functionalized intercalation in normal and inverted organic optoelectronic devices, Light: Sci. Appl. 4 (2015) e273.
[22] B.C. Park, S.H. Yun, C.Y. Cho, Y.C. Kim, J.C. Shin, H.G. Jeon, Y.H. Huh, I.C. Hwang, K.Y. Baik, Y.I. Lee, Surface plasmon excition in semitransparent inverted polymer photovoltaic devices and their applications as label-free optical sensors, Light: Sci. Appl. 3 (2014) e222.
[23] D. Yang, P. Fu, F. j. Zhang, N. Wang, J. Zhang, C. Li, High efficiency inverted polymer solar cells with room-temperature titanium oxide/polyethylenimine films as electron transport layers, J. Mater. Chem. A 2 (2014) 17281–17285.

[24] F. Zhang, M. Ceder, O. Inganäs, Enhancing the photovoltage of polymer solar cells by using a modified cathode, Adv. Mater 19 (2007) 1835–1838.
[25] C.F. Guo, T.S. Sun, F. Cao, Q. Liu, Z.F. Ren, Metallic nanostructures for light trapping in energy-harvesting devices, Light: Sci. Appl. 3 (2014) e161.
[26] Y.Y. He, Z.Q. Li, J.F. Li, X.Y. Zhang, C.Y. Liu, H. Li, L. Shen, W.B. Guo, S.P. Ruan, The role of Au nanorods in highly efficient inverted low bandgap polymer solar cells, Appl. Phys. Lett. 105 (2014) 223305.
[27] C. Yi, R. Hu, H. Ren, X. Hu, S. Wang, X. Gong, Y. Cao, Protonation process of conjugated polyelectrolytes on enhanced power conversion efficiency in the inverted polymer solar cells, J. Photon. Energy 4 (2014) 253–263.
[28] C. Xie, L. Chen, Y. Chen, Electrostatic self-assembled metal oxide/conjugated polyelectrolytes as electron-transporting layers for inverted solar cells with high efficiency, J. Phys. Chem. C 117 (2013) 24804–24814.
[29] B.V.K. Naidu, J.S. Park, S.C. Kim, S.M. Park, E.J. Lee, K.J. Yoon, S.J. Lee, J.W. Lee, Y.S. Gal, S.H. Jin, Novel hybrid polymer photovoltaics made by generating silver nanoparticles in polymer: fullerene bulk-heterojunction structures, Sol. Energy Mater. Sol. Cells 92 (2008) 397–401.
[30] L.L. Huang, X.Z. Chen, B.F. Bai, Q.F. Tan, G.F. Jin, T. Zentgraf, S. Zhang, Helicity dependent directional surface plasmon polariton excitation using a metasurface with interfacial phase discontinuity, Light: Sci. Appl. 2 (2013) e70.
[31] E.D. Kosten, J.H. Atwater, J. Parsons, A. Polman, H.A. Atwater, Helicity dependent directional surface plasmon polariton excitation using a metasurface with interfacial phase discontinuity, Light: Sci. Appl. 2 (2013) e45.
[32] S.I. Na, T.S. Kim, S.H. Oh, J. Kim, S.S. Kim, D.Y. Kim, Enhanced performance of inverted polymer solar cells with cathode interfacial tuning via water-soluble polyfluorenes, Appl. Phys. Lett. 97 (2010) 223305.
[33] S. Khodabakhsh, B.M. Sanderson, J. Nelson, T.S. Jones, Using self-assembling dipole molecules to improve charge collection in molecular solar cells, Adv. Funct. Mater. 16 (2006) 95–100.
[34] G.J. Wang, T.G. Jiu, G. Tang, J. Li, P.D. Li, X.J. Song, F.S. Lu, J.F. Fang, Interface Modification of ZnO-Based Inverted PTB7:$PC_{71}BM$ Organic Solar Cells by Cesium Stearate and Simultaneous Enhancement of Device Parameters, ACS Sustainable Chem. Eng. 2 (2014) 1331–1337.
[35] J. Meyer, S. Hamwi, M. Kroger, W. Kowalshy, T. Riedl, A. Kahn, Transition metal oxides for organic electronics: energetics, device physics and applications, Adv. Mater. 24 (2012) 5408–5427.
[36] Y. Yao, J. Hou, Z. Xu, G. Li, Y. Yang, Effects of solvent mixtures on the nanoscale phase separation in polymer solar cells, Adv. Funct. Mater. 18 (2008) 1783–1789.
[37] H. Hoppe, N.S. Sariciftci, Organic solar cells: An overview, J. Mater. Chem. Research 16 (2011) 1924–1945.
[38] V.D. Mihailetchi, J. Wildeman, P.W.M. Blom, Space-charge limited photocurrent, Phys. Rev. Lett. 94 (2005) 126602.
[39] J.D. Chen, C.H. Cui, Y.Q. Li, L. Zhou, Q.D. Ou, C. Li, Y.F. Li, J.X. Tang, Single-junction polymer solar cells exceeding 10% power conversion esfficiency, Adv. Mater 27 (2015) 1035–1041.
[40] B. Kan, M.M. Li, Q. Zhang, F. Liu, X.J. Wan, Y.C. Wang, W. Ni, G.K. Long, X. Yang, H. R. Feng, Y. Zuo, M.T. Zhang, F. Huang, Y. Cao, T.P. Russell, Y.S. Chen, A series of simple oligomer-like small molecules based on oligothiophenes for solution-processed solar cells with high efficiency, J. Am. Chem. Soc. 137 (2015) 3886–3893.
[41] S.W. Tsang, S.C. Tse, K.L. Tong, S.K. So, PEDOT: PSS polymeric conducting anode for admittance spectroscopy, Org. Electron. 7 (2006) 474–479.
[42] S.W. Tsang, S.K. So, J.B. Xu, Application of admittance spectroscopy to evaluate carrier mobility in organic charge transport materials, J. Appl. Phys. 99 (2006) 013706.
[43] X. Chen, B.H. Jia, Y.A. Zhang, M. Gu, Exceeding the limit of plasmonic light trapping in textured screen-printed solar cells using Al nanoparticles and wrinkle-like graphene sheets, Light: Sci. Appl. 2 (2013) e92.